

# Charge Carrier Localization and Transport in Organic Semiconductors: Insights from Atomistic Multiscale Simulations

Marko Mladenović and Nenad Vukmirović\*

Organic electronic semiconducting materials exhibit complex atomic structures with a lack of periodicity that lead to charge carrier localization which, in turn, strongly affects the electronic transport properties of these materials. To understand charge carrier localization and electronic transport in organic semiconductors, simulations that take into account the details of the atomic structure of the material are of utmost importance. In this article, computational methods that can be used to simulate the electronic properties of organic semiconductors are reviewed and an overview of the results that have been obtained from such simulations is given. Using these methods the effects of static disorder, thermal disorder and interfaces between domains are investigated and the microscopic origin of these effects is identified. It is shown that in strongly disordered conjugated polymer materials the main origin of the localization of charge carrier wave functions is the disordered long-range electrostatic potential. In ordered polymers, thermal disorder of main chains leads to wave function localization. In small molecule based organic semiconductors, grain boundaries introduce localized trap states at the points where electronic coupling is the strongest. It is also demonstrated that detailed atomistic simulations are necessary for quantitative and sometimes even qualitative description of charge mobility in organic materials.

## 1. Introduction

Organic semiconductors based on conjugated polymers and small molecules have emerged in the last two decades as materials with applications in sensing, lighting, displays, solar energy conversion, and so forth.<sup>[1–10]</sup> Their main advantage is a significantly lower production cost in comparison to their inorganic counterparts.<sup>[11]</sup> Organic materials obtained by standard processing techniques exhibit a wealth of structures,<sup>[12–14]</sup> including completely disordered spaghetti-like regions formed by interlaced chains of conjugated polymers,<sup>[15]</sup> ordered regions of polymer chains arranged in two-dimensional lamellar structures,<sup>[16,17]</sup> polycrystalline small molecule-based structures<sup>[18–21]</sup>

and small molecule-based single crystals.<sup>[22,23]</sup> The variety of organic semiconductors, their possible morphologies and the complexity of these morphologies make understanding of their electronic properties a rather challenging task. One cannot exploit the well developed theory of inorganic crystalline semiconductors where charge carriers are fully delocalized Bloch waves whose transport is limited by occasional scattering on phonons, defects or impurities.

On the other hand, a common feature of almost all organic semiconductors is the localization of charge carriers at band edge energies which arises due to a certain type of disorder in the material. In this feature article, we will discuss and quantify various effects of disorder that lead to charge carrier localization. We will also discuss the consequences of charge carrier localization on electrical transport properties of these materials.

To reliably calculate the wave functions and their localization properties in disordered organic semiconductors, the

calculations on the length scale larger than the wave function localization length are necessary. This implies the length on the order of several nanometers, which encompasses several thousand atoms. Such a number of atoms is beyond what is achievable by standard density functional theory (DFT) based calculations. Consequently, the need for understanding the electronic properties of organic semiconductors has stimulated the development of methods for electronic structure calculations. These methods will be described in Section 3. Before describing these methods and the insights obtained from their applications to organic semiconducting materials, we will introduce a toy model of an organic semiconductor in Section 2. This model will be very helpful to qualitatively understand the essence of most effects obtained from detailed atomistic simulations. Section 4 is devoted to the overview of insights obtained from atomistic simulation about the electronic properties of the material, such as the wave function localization and the electronic density of states (DOS). In Section 5, we present insights into the electrical transport in amorphous polymers obtain from the simulations and briefly discuss possible insights into the electrical transport of other classes of organic semiconductors.

M. Mladenović, Dr. N. Vukmirović  
Scientific Computing Laboratory  
Institute of Physics Belgrade  
University of Belgrade  
Pregrevica 118  
11080 Belgrade, Serbia  
E-mail: nenad.vukmirovic@ipb.ac.rs



DOI: 10.1002/adfm.201402435

## 2. A Toy Model Hamiltonian of an Organic Semiconductor

We model the electronic Hamiltonian of the states near the top of the valence band (or the bottom of the conduction band) as

$$H = \sum_{i=1}^{N_c} H_i + \sum_{i=1}^{N_c} \sum_{j=1}^{i-1} H_{ij} \quad (1)$$

where

$$H_i = \sum_{j=1}^{L_i} \varepsilon_{ij} a_{ij}^{\dagger} a_{ij} - \sum_{j=1}^{L_i} \sum_{k=1}^{j-1} t_{i,j,i,k} (a_{ij}^{\dagger} a_{ik} + a_{ik}^{\dagger} a_{ij}) \quad (2)$$

and

$$H_{ij} = - \sum_{m=1}^{L_i} \sum_{n=1}^{L_j} t_{i,m;j,n} a_{im}^{\dagger} a_{jn} \quad (3)$$

In Equations 1–3  $N_c$  is the total number of polymer chains,  $L_i$  is the length (number of monomers) of polymer chain  $i$ ,  $\varepsilon_{ij}$  is the on-site energy of the monomer  $j$  on chain  $i$ ,  $t_{m,j;n,k}$  are the electronic coupling elements between the monomer  $j$  on chain  $m$  and the monomer  $k$  on chain  $n$ , while  $a_{ij}$  and  $a_{ij}^{\dagger}$  are the carrier annihilation and creation operators on site  $j$  in chain  $i$ . This Hamiltonian is flexible enough to provide insight into various classes of organic materials as will be discussed below. Schematic illustration of the parameters of the Hamiltonian is presented in **Figure 1a**.

Ideally ordered polymer regions (**Figure 2e**) consist of two dimensional planes of parallel aligned chains.<sup>[24–28]</sup> In the chain direction, the monomers are bonded by covalent bonds which lead to strong electronic coupling. In the direction in the planes perpendicular to the chain direction ( $\pi$ – $\pi$  stacking direction), the chains are bonded by weak van der Waals interaction and electronic coupling in that direction is still sufficient to cause delocalization of electronic wave function. In the third direction the planes are separated by insulating alkyl side chains which lead to completely negligible electronic coupling and conduction. Consequently, ordered polymers can to a first approximation be modeled by taking all chain lengths to be equal  $L_i = \text{const}$ , by assuming equal nearest neighbor intrachain electronic coupling elements  $t_{i,j;i,j+1} = t_1$  and by taking the interchain coupling elements between neighboring monomers from different chains equal to another constant  $t_{i,j;i+1,j} = t_2$ , while the remaining coupling elements are assumed to be equal to zero. The value of  $t_1$  in conjugated polymers can be estimated as half the bandwidth of HOMO (or LUMO) band of a straight polymer chain. These bandwidths are typically on the order of 2 eV (see the literature<sup>[29]</sup> for the cases of polythiophene, polyfuran and polypyrrole), which leads to the estimate for  $t_1$  of 1 eV. On the other hand, the value of  $t_2$  can be estimated from the bandwidth in the  $\pi$ – $\pi$  stacking direction, which is on the order of 0.2 eV (see another study for the case of polythiophenes)<sup>[28]</sup> and gives an estimate for  $t_2$  of 0.1 eV.

In strongly disordered polymers, the chains form a spaghetti-like structure (**Figure 2d**). The origin of such a shape of the chains is the fact that the energy required to rotate the monomers around the bond that connects them is comparable



**Marko Mladenović** is Research Assistant at the Institute of Physics Belgrade. His research interests are electronic and transport properties of organic semiconductors. He obtained his MSc degree in nanoelectronics and photonics at the School of Electrical Engineering, University of Belgrade in 2012. Currently, he is a PhD student working under the supervision of Dr. Nenad Vukmirović. He is the recipient of the 2014 E-MRS Graduate Student Award.



**Dr. Nenad Vukmirović** is Associate Research Professor at the Institute of Physics Belgrade. His research interests are theory and simulation of electronic properties of organic semiconductor materials and quantum nanostructures. He received his BSc degree in physics in 2003 and in electrical engineering in 2004, both from the University of Belgrade.

He received his PhD degree in electrical engineering in 2007 from University of Leeds, UK. From 2007 to 2010 he was a postdoctoral fellow at Lawrence Berkeley National Laboratory. Dr. Vukmirović is holder of the FP7 Marie Curie Career Integration Grant for the project Electronic Transport in Organic Materials.

to thermal energy. Such rotations lead to irregular shape of the chain. It is important to note that the chains keep their shape on a time scale of at least a nanosecond.<sup>[30]</sup> This timescale is longer than the timescale relevant for charge transport processes. Therefore the disorder introduced by the irregular shape of the chains is called the “static disorder”. The effects of static disorder are reflected both in the on-site energies and in the electronic coupling elements in the Hamiltonian that are no longer constant but vary in space in a largely random manner. In a disordered polymer material the monomer experiences the electrostatic potential from charges on all other monomers. Since the orientations of these monomers are largely random, the potential they create is also random and this leads to variations of monomer on-site energies. On the other hand, the electronic coupling between the neighboring monomers is mostly determined by their mutual orientations. It is well understood that the overlap of  $\pi$  orbitals strongly depends on the angle between them. In a typical chain in disordered polymers, the angles between monomers take largely random values, which leads to variations of intrachain nearest neighbor electronic coupling elements. Therefore, the static disorder in amorphous polymers is reflected through variations of on-site elements in Equation 2 caused by random electrostatic potential

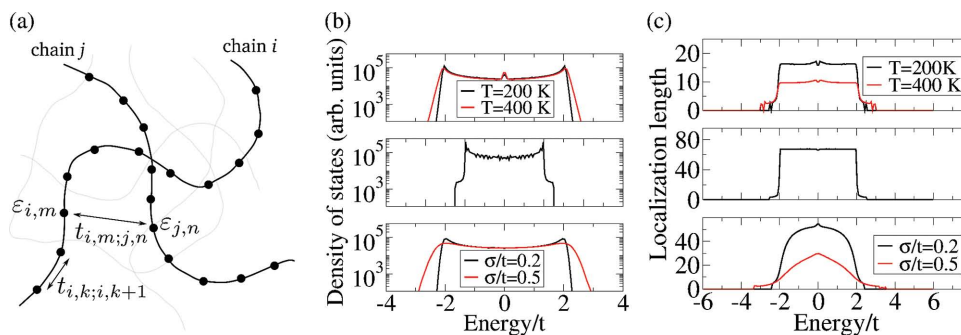


**Figure 1.** a) Schematic representation of disordered polymer morphology and relevant parameters of the toy model Hamiltonian. b) Electronic DOS and c) the localization length for one dimensional model with Gaussian disorder (bottom), model of a grain boundary (middle) and model of an organic crystal (top).

and through variations of electronic coupling elements in Equation 2,3 caused by rotations of the monomers around the bonds that connect them.

The Hamiltonian which is representative of small molecule based organic crystals (Figure 2f) can be obtained if one assumes that  $L_i = 1$  and that  $t_{i,j,1} = t_2$  for molecules which are nearest neighbors. Typical values of  $t_2$  are on the order of 50 meV.<sup>[31,32]</sup> Such a Hamiltonian at first sight exhibits no effects of disorder because all the parameters of the Hamiltonian are constant and the system is perfectly periodic. However, a characteristic feature of organic materials is that the oscillations of atoms around their equilibrium positions at finite temperature are significant due to softness of intermolecular van der Waals bonds.<sup>[33]</sup> Each of the parameters of the Hamiltonian depends on atomic positions. At a certain moment in time, the atomic positions are not periodic and the parameters of the Hamiltonian take values that vary through space in a random manner. Such a disorder introduced by oscillations of atoms around their equilibrium positions is called the dynamic disorder or thermal disorder. In small molecule based crystals, the variations of  $t_{i,j,1}$  are comparable to its mean value.<sup>[33,34]</sup>

The proposed model can also account for the effects of grain boundaries in organic crystals, through the changes in electronic coupling elements at the grain boundary.

Thermal disorder is also present in polymer based materials. In strongly disordered polymers it is an additional component of disorder that comes on top of strong static disorder and is therefore of secondary importance. However, in ordered polymer regions it is of major importance since it is the only type of disorder.

In this article, we will not take into account possible effects of polarons on the properties of organic semiconductors. The polarons are quasiparticles formed from a charged particle and the surrounding cloud of atomic displacements induced by the presence of the charged particle which lower the energy of the particle. In the Hamiltonian given by Equation 1–3 polaronic effects could be modeled by taking into account the dependence of the parameters on the atomic coordinates and by adding an additional term with the dependence of the energy of the neutral system on atomic coordinates. There is recent evidence in the literature that in several types of organic semiconductors the effects of polarons might not be as important

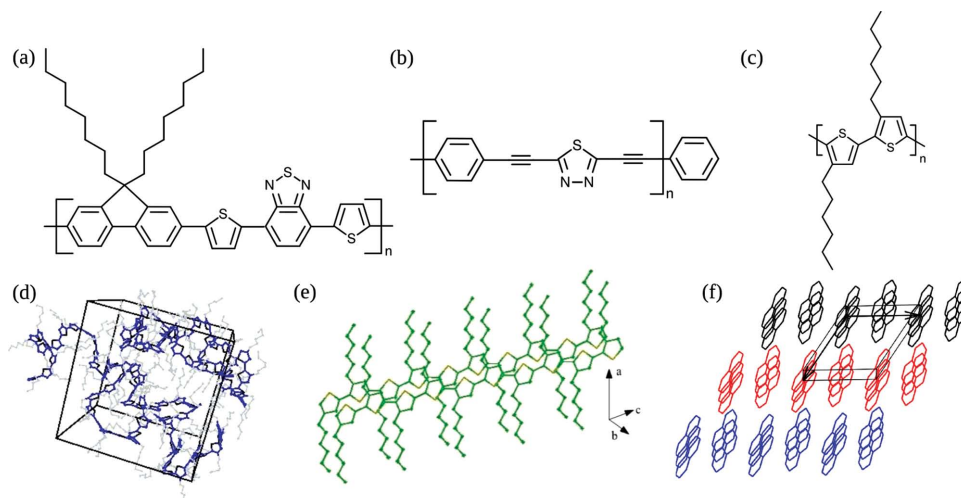


**Figure 2.** Chemical formulae of conjugated polymers mentioned in this article: a) poly[2,7-(9,9-dioctyl-fluorene)-alt-5,5-(4',7'-di-2-thienyl-2',1',3-benzothiadiazole)] (APFO-3); b) 2,5-bis(phenylethynyl)-1,3,4-thiadiazole (PhEtTh); c) poly(3-hexylthiophene) (P3HT) and atomic structures of several classes of organic semiconductors: d) disordered polymers; e) ordered polymers; f) small molecule based crystals.

as previously thought. The results of DFT calculations of long straight polythiophene chains have indicated that polaron binding energy is on the order of few meVs only and that it can be ignored in practice.<sup>[35,36]</sup> It has been argued elsewhere<sup>[37]</sup> that small polaron formation does not take place in oligoacenes such as pentacene and rubrene. Our calculations point out to the same conclusion for pentathiophene monolayers<sup>[38]</sup> and naphthalene crystals.<sup>[39]</sup> It is more difficult to assess the effect of polarons in disordered materials because of the lack of theoretical framework that is capable of accounting for the effects of disorder and polarons on equal footing in realistic materials. Nevertheless, one may argue that if the strength of disorder (quantified for example by the magnitude of spatial variations of onsite elements in the Hamiltonian) is larger than the monomer polaron binding energy, the effects of disorder would have a major influence on the electrical properties of the material. In this article we focus on the effects of localization caused by static or dynamic disorder and show that these are sufficient to lead to significant localization of band edge wave functions without the polaronic effects. On the other hand, further understanding of the role of polarons in organic materials is certainly desirable.

### 3. Methods for Electronic Structure Calculations

In this section, the methods that can be used in practice to calculate the electronic structure of organic semiconductors will be briefly described.

Atomic structure of the material is needed as an input for electronic structure calculations. In the studies of thermal disorder in ordered materials one starts with an ideal room temperature crystal structure and then evolves the system in time using molecular dynamics (MD) technique or samples various possible atomic configurations using a configurational Monte Carlo (MC) approach.<sup>[40]</sup> After the equilibration of the system takes place, one continues with the production run where uncorrelated snapshots of the atomic configuration of the system are extracted for further use in electronic structure calculations. To obtain the atomic structure of amorphous material, a more elaborate approach is needed. This is accomplished using a simulated annealing procedure. Initially, polymer chains are placed in a box which is much larger than the one that corresponds to experimental density of the material and a high temperature of 1000 K is imposed. The size of the box is then gradually decreased during the MC or MD simulation until it reaches the final size that corresponds to experimental density of the material. Finally, the temperature is also gradually decreased down to room temperature and the system is relaxed to a local minimum. The procedure of this type was established as a standard procedure for the generation of the atomic structure of amorphous polymers.<sup>[41–47]</sup> While such procedures are typically applied in simulations of amorphous polymers, one should keep in mind that the atomic structures obtained are only models that are constructed to capture the features of fully disordered polymer materials. It is well established from experiments that the polymer molecular weight affects the order in the structures and that realistic materials contain both ordered and disordered regions. It is a challenging

task that is beyond of the scope of this article to obtain the atomic structure of polymer based materials in such cases.

After obtaining the atomic structure of the material, electronic structure calculations can be performed. This can be done, in principle, using DFT.<sup>[48]</sup> Within DFT, Kohn-Sham equations for wave functions of all occupied electronic states have to be solved self-consistently. Due to its significant computational cost, this approach is typically practiced only for systems with less than a thousand atoms which is usually not sufficiently large size to obtain reliable information about the properties of disordered materials.

Charge patching method (CPM)<sup>[49]</sup> can be used to directly calculate the electronic charge density. This method is based on the assumption that the contribution of a particular atom to the total electronic charge density of the system depends mainly on its local environment. Such contributions are called motifs and these are extracted from a DFT calculation of a small prototype system where atoms have the same bonding environment as in the simulated system. Contribution of an atom A at a position  $\mathbf{R}_A$  is given as<sup>[49]</sup>

$$m_A(\mathbf{r}-\mathbf{R}_A) = \frac{w_A(\mathbf{r}-\mathbf{R}_A)}{\sum_B w_B(\mathbf{r}-\mathbf{R}_B)} \rho(\mathbf{r}) \quad (4)$$

where  $\rho(\mathbf{r})$  is the electronic charge density obtained from DFT calculation on the small prototype system, while  $w_A$  is the weight function of an atom A. The total electronic charge density of the large system that one wants to simulate is then calculated as a sum of contributions of motifs corresponding to each atom in the system. When charge density is known, the single-particle Hamiltonian can be constructed as

$$H = -\frac{\hbar^2}{2m_0} \nabla^2 + v_l + \frac{e}{4\pi\epsilon_0} \int \frac{\rho(\mathbf{r}')}{|\mathbf{r}-\mathbf{r}'|} d^3\mathbf{r}' + v_{xc}^{\text{LDA}}(\rho) \quad (5)$$

where the first term is the kinetic term, the second term is the potential of core ions, the third term is the electrostatic (Hartree) potential, while the last term is the exchange-correlation term calculated using local density approximation (LDA) within DFT. The Hamiltonian obtained using CPM gives an accurate approximation of the DFT/LDA Hamiltonian for systems where there is no long range charge transfer with typical eigenenergy errors on the order of tens of meV.<sup>[49]</sup>

To describe electrical transport properties of a semiconducting material, only spectral region in the vicinity of the band gap is relevant. Therefore it is not necessary to find all eigenvalues of the Hamiltonian given by Equation (5). Instead, one can find the eigenstates closest to a certain reference energy using the folded spectrum method (FSM).<sup>[50,51]</sup> The main idea of the method is to solve the eigenvalue problem of the operator  $(H - E_{\text{ref}})^2$ . Lowest eigenstates of this operator correspond to the eigenstates of the operator  $H$  closest to reference energy  $E_{\text{ref}}$ . With a proper choice of  $E_{\text{ref}}$  one can find the relevant states at the bottom of the conduction band or the top of the valence band.

For a system containing a large number of atoms, the use of FSM for the diagonalization of the Hamiltonian represented in plane wave basis may become too computationally demanding. Instead of using plane waves as the basis set, the Hamiltonian

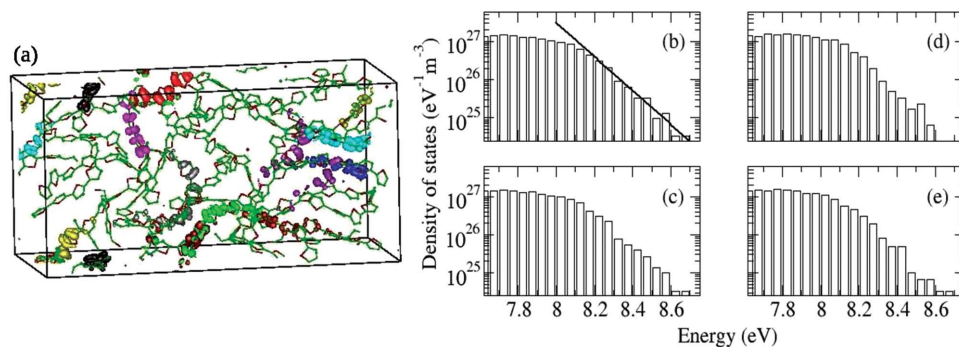


**Figure 3.** a) Wave functions moduli squared of top ten hole states in the portion of amorphous P3HT material of the size  $58.6 \times 29.3 \times 29.3 \text{ \AA}^3$ . The isosurfaces correspond to the 50% probability of finding the hole inside the surface. b) The hole DOS in amorphous P3HT material obtained from the full calculation; c) in the absence of interchain electronic coupling; d) calculated by including the intrachain electronic coupling between the nearest neighbors only; e) calculated by assuming that the intrachain electronic coupling between nearest neighbors is constant and equal to  $t = 0.85 \text{ eV}$ .

can be represented in a localized and physically motivated system specific basis set. Overlapping fragments method (OFM)<sup>[52]</sup> is an efficient method which is based on the division of the system into small fragments and the use of eigenvectors of the fragments as the basis set. Good representation of relevant electronic states is obtained when the fragments mutually overlap. To achieve sufficient accuracy, only a few states per fragment are needed. OFM is particularly suitable for systems in which division into fragments is natural, such as conjugated polymers.

Several other methods have also been applied in the literature to calculate the electronic structure of large portions of organic materials—these include the density functional tight-binding method,<sup>[53]</sup> localized molecular orbital method,<sup>[54]</sup> and sometimes even direct DFT calculation<sup>[42]</sup> which however puts a severe restriction on the size of the system that can be tackled with available computational resources.

#### 4. Localization and the Density of States

The effects of disorder discussed in Section 2 lead to localization of band edge wave functions and to the tail in the electronic

DOS at the spectral region near the band edge. Grain boundaries introduce the wave functions localized at the boundary whose energies are within the band gap of the bulk semiconductor. In this section we present the densities of states and the localization lengths obtained from detailed atomistic simulations and provide insight into the origin of the results obtained with the help of a toy model presented in Section 2.

##### 4.1. Amorphous Polymers

The wave functions and energies of electronic states in the region near the top of the valence band in the amorphous P3HT polymer (whose chemical formula is given in Figure 2c) were calculated using the CPM and OFM, as described in Section 3. The calculations have been performed for 50 different realizations of the system that consists of 12 chains, each 40 thiophene units long.<sup>[55]</sup> Such a system has 12024 atoms altogether. The electronic DOS near the top of the valence band obtained from such a set of calculations is presented in Figure 3b, while the dependence of localization length on energy is shown in Figure 4a. The localization length  $L$  was calculated as  $L = 1 / \sum_m |d_m|^4$ , where  $d_m$  are expansion

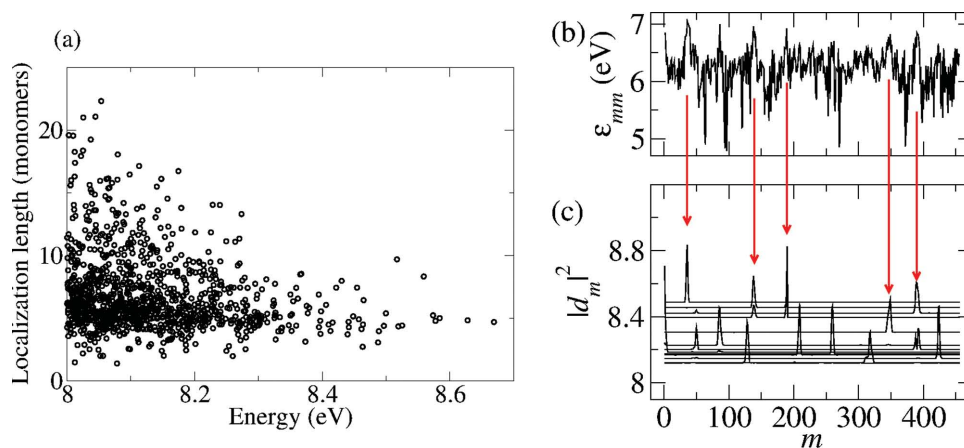


**Figure 4.** a) Dependence of localization length on energy in amorphous P3HT polymer; b) On-site Hamiltonian matrix elements  $\epsilon_{mm}$  (where  $m$  is the index of the site on the polymer chain) for one realization of 12 024 atom P3HT polymer system; c) The wave functions of top hole states in 12024 atom P3HT system.  $|d_m|^2$  are moduli squared in the expansion of the wave function in an orthonormal basis set shifted by the energy of the hole state in eV.

coefficients of the wave function in the orthonormal and localized basis  $|m\rangle$ . Strictly speaking, this quantity is in literature called the inverse participation ratio (IPR) and can be thought of as the number of monomers that the wave function is localized on. When IPR is multiplied by the length of one monomer it gives us the information about the length of the region of space where the wave function is localized. For this reason, IPR can also be thought of as the localization length where the unit of length is the length of one monomer. In the rest of this article IPR will be referred to as the localization length. The results indicate that electronic states near the valence band edge are strongly localized, while as one goes away from the band edge more delocalized states start to appear. The DOS exhibits a tail which can be well fitted with an exponential function, as shown in Figure 3b. As discussed in detail in the literature,<sup>[55]</sup> the best fit with an exponential function gives 84% confidence that the distribution is exponential, while the fits using a Gaussian function give the confidence of 16% or less.

To understand different effects in the system, we have mapped the Hamiltonian obtained from the CPM and OFM to the form of the Hamiltonian discussed in Section 2 by using the Lowdin's orthonormalization procedure, as discussed in detail elsewhere.<sup>[55]</sup>

#### 4.1.1. The Origin of Localization

A picture that is often used to understand the localization of wave functions in conjugated polymers is so called conjugation break model. Within such a picture the wave functions are delocalized along the planar parts of the polymer chain where electronic coupling between the monomers is strong. The places where the torsion angle between the monomers is larger than some critical value break the conjugation and localize the wave function. The simplest mathematical description of the conjugation break model is the special case of the toy model outlined in Section 2 where on-site elements are constant and nearest neighbor coupling elements are constant as well, except that at the places where the conjugation break takes place they take the zero value. Within such a model the wave functions at the band edge would have the largest localization length, while the states further away from the band edge would be more localized. These results suggest that the simple conjugation break model is not appropriate for the description of amorphous polymers as it yields a completely different behavior of the dependence of localization length on energy than the one obtained from atomistic simulations. The main origin of this is the absence of variations of on-site Hamiltonian matrix elements caused by disordered electrostatic potential, which is known to be important in organic materials.<sup>[47,56,57]</sup>

On the other hand, the localization of band edge states is well known from the theory of one-dimensional disordered systems.<sup>[58]</sup> For example, a system described by our toy model Hamiltonian with constant nearest neighbor electronic coupling elements and with onsite elements drawn from a Gaussian distribution yields the dependence of localization length on energy which is qualitatively similar to the dependence that we obtain. However, a more detailed investigation is

required to understand the origin of the dependence of localization length that we obtain and to establish if the results obtained can be really related to the results of disordered one-dimensional systems.

On that route, one first has to establish if the polymer material can in certain sense be considered simply as a collection of independent polymer chains. In Section 2, we have discussed that interchain electronic coupling in ordered polymers is an order of magnitude smaller than the intrachain coupling. In amorphous polymers where the spatial region between the main chains is also filled by insulating side chains, it is expected that interchain electronic coupling is even less important since it may have significant values only at certain points in space where parts of two main chains are closely stacked. To check if this is really the case, we have excluded interchain electronic coupling from the calculation. The DOS obtained without interchain electronic coupling is presented in Figure 3c. By comparing Figure 3b and Figure 3c it is evident that the effect of interchain coupling on electronic DOS is very small. The same is the case for the dependence of localization length on energy (not shown) which changes only slightly in the absence of interchain electronic coupling. One should note that these results do not suggest that interchain electronic coupling is irrelevant in organic materials. In Sections 4.2. and 4.3. we demonstrate the important role of interchain or intermolecular electronic coupling in the formation of electronic states in ordered polymers and at grain boundaries between small molecule based crystals. In addition, when electrical transport is concerned, long-range transport is impossible without interchain coupling which is required for charge transfer between different chains.

Next, to simplify the Hamiltonian, we exclude all intrachain electronic coupling elements except the ones between nearest neighbors. The comparison of Figure 3b and Figure 3d indicates that this is a good approximation. Finally, we set all nearest neighbor electronic coupling elements to a constant value  $t = 0.85$  eV which corresponds to the most probable value in the distribution of these elements. Even such a drastic change has a weak effect on electronic DOS, as seen by comparing Figure 3b and Figure 3e. Such a result shows that the Hamiltonian which includes only on-site elements and constant nearest neighbor intrachain coupling elements captures the main features of the electronic states near the band edge, including their localization properties. Consequently, the variations of on-site elements that originate from disordered electrostatic potential introduced from the rest of the system are responsible for localization of wave functions rather than the breaks in conjugation. This conclusion can further be supported from Figure 4b,c. The hole wave functions are localized precisely at the places of largest on-site elements in agreement with the notion that these elements are responsible for localization.

#### 4.1.2. The Factors that Influence the Electrostatic Disorder

Given the established importance of the disordered electrostatic potential created by the rest of the system on a certain site, it is of great relevance to understand the factors that determine the degree of spatial variations of such a potential. In typically used conjugated polymers there is always some degree

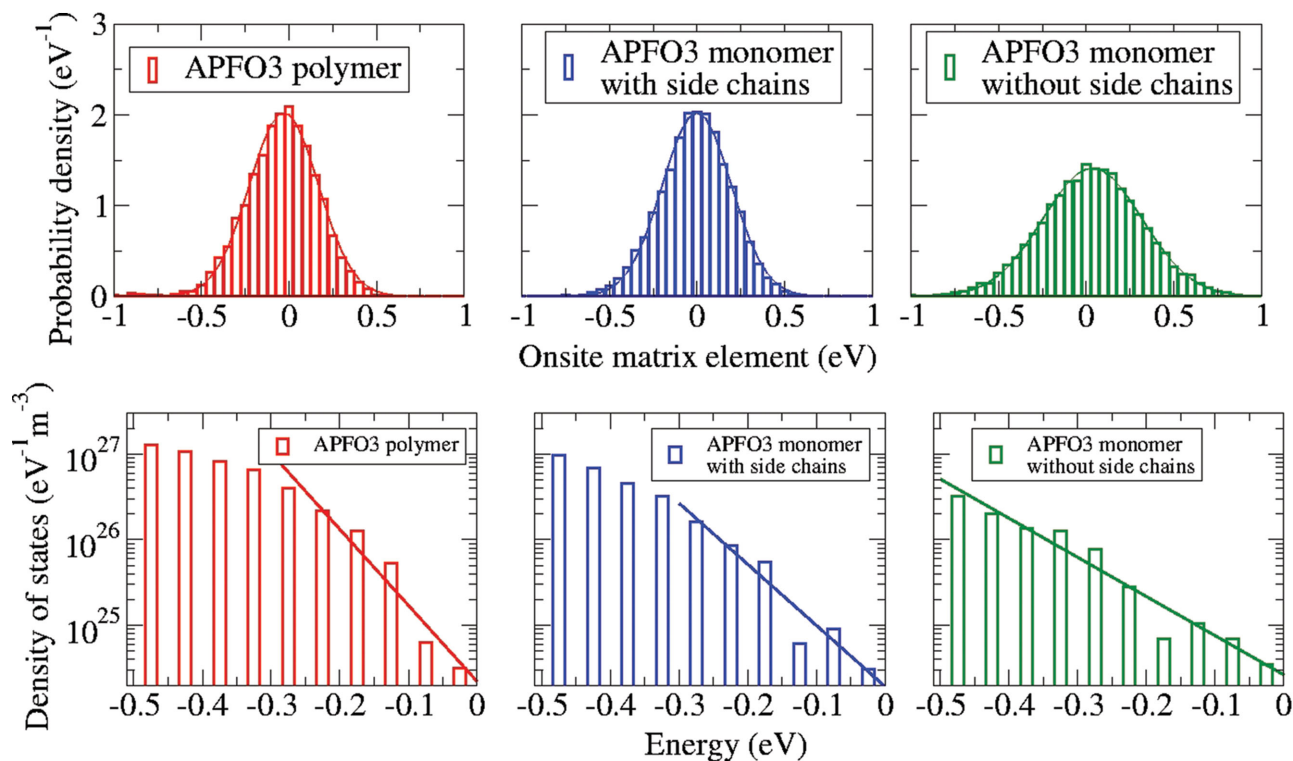


**Figure 5.** The distribution of on-site matrix elements for several materials based on APFO-3 (top). The lines are best fits to the Gaussian distribution with the standard deviation parameter  $\sigma = 197$  meV (APFO-3 polymer),  $\sigma = 197$  meV (APFO-3 monomer with side chains), and  $\sigma = 282$  meV (APFO-3 monomer without side chains). The density of hole states for these materials (bottom). The lines represent fits to the exponential DOS  $D(E) = D_0 \exp(-E/E_b)$ , with  $E_b = 48.9$  meV for APFO-3 polymer,  $E_b = 60.9$  meV for APFO-3 monomer with side chains and  $E_b = 95.1$  meV for APFO-3 monomer without side chains.

of charge transfer in the monomer. Consequently, from the electrostatic point of view, each monomer can be considered as a dipole that creates a long-ranged electrostatic potential. Since the polymers have irregular shape, the orientations of these dipoles vary and there is a great degree of randomness in the overall potential created by these dipoles. The strength of the electrostatic potential on a certain site depends both on the strength of the dipoles and on their distances from the site. For this reason, one expects that alkyl side chains that act as spacers between the main chains tend to reduce the electrostatic disorder.

To investigate the effects of electrostatic disorder in more detail, we consider three systems based on APFO-3 polymer (whose chemical formula is given in Figure 2a), the APFO-3 polymer with side chains, the APFO-3 monomer with side chains, and the APFO-3 monomer without side chains.<sup>[59]</sup> The monomer of APFO-3 is in a donor–acceptor–donor configuration which leads to the creation of dipoles within the monomer. For this reason, it is an interesting material for the study of electrostatically induced disorder. To quantify the electrostatic disorder, we present the distribution of diagonal Hamiltonian matrix elements  $H_{ii}$ , where  $i$  is the fragment orbital. The distribution of these elements in the case of APFO-3 polymer with side chains and APFO-3 monomer with side chains is presented in Figure 5. These distributions are nearly the same which is an expected result since both systems have the same built-in dipoles in the monomer and the same distribution of

distances between the sites on the main chain and the dipoles. In addition, the distribution of torsion angles in both systems is rather similar which leads to similar distribution of the dipoles orientation. On the other hand, the comparison of the APFO-3 monomer with and without side chains (also shown in Figure 5) yields a wider distribution of elements in the monomer without side chains. The origin of wider distribution is the absence of side chains, which leads to proximity of the surrounding dipoles and consequently to a stronger and more disordered potential.

Next, we compare the DOS of the three materials, shown in Figure 5. It is expected that the material with wider distribution of diagonal matrix elements has a wider tail in the DOS at the band edge. Indeed, as seen from the fit of the DOS to an exponential function presented in Figure 5, APFO-3 monomer without side chains has significantly larger  $E_b$  than the other two materials. The comparison of APFO-3 polymer and APFO-3 monomer with side chains yields somewhat smaller  $E_b$  in APFO-3 polymer. These two materials have the same distribution of diagonal elements, while the smaller  $E_b$  in APFO-3 polymer comes from tail narrowing introduced by intrachain electronic coupling in the polymer.<sup>[59]</sup>

#### 4.1.3. Impact of Electrostatic Disorder on the Band Gap

The effect of disordered electrostatic potential may be so pronounced in some materials to even lead to a drastic reduction

of the band gap. One such material is PhEtTh (whose chemical formula is given in Figure 2b).<sup>[60]</sup> The calculation of the amorphous PhEtTh sample, consisting of 5 decamers (1010 atoms) yields the bandgap of 0.62 eV. On the other hand, the band gap of an isolated straight PhEtTh chain is 1.64 eV, while the band gaps of isolated chains in the amorphous geometry take the values in the 1.60–1.85 eV range. One should note that these band gaps were obtained from the calculation based on the LDA approximation and are therefore underestimated in comparison to true band gaps. Nevertheless, here we are mainly interested in the change of the band gap from straight polymer single chain to amorphous material and we are not focused on the absolute values of the band gap. The reader interested in the absolute value of the band gap may estimate it by dividing the LDA gap with a factor of 0.6.<sup>[60]</sup>

The directly calculated interchain coupling elements in amorphous PhEtTh take the values on the order of 10 meV and these certainly cannot explain the difference between the band gaps of the material and the individual chains. To understand this band gap difference, we have performed the calculations where we have represented the Hamiltonian in the basis of eigenstates of single chains. In this basis certain coupling elements can be easily turned on and off and therefore their influence on the electronic structure can be identified. First, we represent the Hamiltonian in this basis and do not turn any elements off. We obtain the band gap of 0.79 eV, somewhat different than the band gap obtained by plane wave diagonalization. This difference originates from the incompleteness of the basis set used. However, this difference is not large and therefore this basis set can be used to understand the role of different coupling elements. Next, the interchain coupling elements of the Hamiltonian  $H - H_s$  (where  $H$  is the Hamiltonian of the whole system, while  $H_s$  is the sum of Hamiltonians of individual isolated chains) between the eigenstates of single chains were turned off and the band gap obtained is 0.8 eV. Then, we also turn off the intrachain off-diagonal coupling elements and obtain the band gap of 1.01 eV. Finally, when onsite term is also ignored we obtain the single chain band gap of 1.6–1.85 eV.

From these calculations, we can identify the relative importance of various factors in determining the band gap of the system. Individual chains have band gaps in the 1.6–1.85 eV region. Other chains create an additional potential on each chain which changes the onsite energies and leads to the reduction of the band gap to 1.01 eV. This potential also mixes different states from a particular chain, which leads to further band gap reduction to 0.8 eV. Finally, interchain electronic coupling has a rather weak effect and only slightly reduces the band gap to 0.79 eV.

Such a drastic effect of electrostatic potential on the band gap was not obtained in polythiophene polymers<sup>[41]</sup> with or without side chains. The main difference between polythiophene and PhEtTh materials lies in the fact that the monomer of PhEtTh, which is a donor acceptor copolymer, has a significant dipole moment that originates from the charge transfer of 0.14 electrons from thiadiazole to benzene ring. On the other hand, such a strong dipole moment is not present in polythiophenes. These dipoles then introduce long range electrostatic potential which is responsible for band gap reduction.

Reduction of the band gap by electrostatic disorder can be understood from a simple one dimensional model (which is a special case of the toy model from Section 2) where on-site energies have a Gaussian distribution with standard deviation  $\sigma$  and electronic coupling  $t$  is present between nearest neighbors only. In Figure 1b,c (bottom panel) we present the DOS and the localization length (obtained by averaging of 25 000 different realizations of the system consisting of 100 sites) for such a model for two values of the  $\sigma/t$  ratio. As seen from the figure, when this ratio increases, localized states deeper in the band gap start to appear and consequently the band gap is reduced. However, one should have in mind that polymers where this effect is pronounced also have a rather poor mobility due to wide DOS tail and are therefore not suitable for any practical applications in electronics. Consequently, for electronic applications one should generally avoid polymers with strong built-in dipole moments within the monomer.

## 4.2. Thermal Disorder in Ordered Conjugated Polymers and Small Molecules

As pointed out in Section 2, the effects of thermal disorder may be significant in ordered conjugated polymer materials. This expectation comes from the weakness of interchain van der Waals bonding and the possibility of monomer rotation around the bonds that connect them (torsions) at finite temperature. Thermal disorder in ordered conjugated polymer materials originates both from disorder in the shape of main (backbone) chains and alkyl side chains. Wave functions of relevant electronic states are localized dominantly on the main chains. Therefore, disorder in main chains, which includes variations in torsion angles between thiophene rings and the displacements of the entire chains, directly affects the localization length of wave functions. On the other hand, the effect of side chains on the electronic structure is not that transparent. Disorder in the shape of side chains produces spatial variations of the electrostatic potential on the main chains, which subsequently affect the electronic structure.

The effects of thermal disorder on electronic structure of crystalline region of P3HT were investigated using the atomic structures of P3HT at a temperature of 300 K generated from MC simulations. Crystalline P3HT may exhibit the structure where main chains are aligned and the structure where these are mutually shifted by half a unit cell length in the main chain direction.<sup>[24]</sup> Below we will show the results for the shifted structure which is more energetically favorable,<sup>[24]</sup> while one expects qualitatively the same results for the aligned structure.

The isolated effect of disorder in side chains was investigated first by keeping main chains rigid during MC simulations. Then, the simulations were repeated allowing disorder in main chains as well. During the simulations the bond lengths and bond angles were kept constant, since their variations have only a slight effect on the electronic structure. Electronic structure calculations were performed using the CPM and the OFM. Small molecules consisting of three neighboring thiophene rings (trimers) were used as fragments in the OFM.

Effects of thermal disorder on electronic structure of P3HT were quantified by calculating the DOS and the wave function

localization length for ten highest states in the valence band, which cover the relevant spectral region of around 0.5 eV. The calculation was repeated for 100 different random realizations of the atomic positions for the system that consists of 10 chains, each 10 thiophene rings long.

Electronic DOS, total localization length and the localization length in the  $\pi$ - $\pi$  stacking direction for the structures with disorder in side chains only and disorder in both main and side chains are shown in **Figure 6**. Results indicate that disorder in side chains has a relatively weak effect on the electronic structure. In this case, DOS contains several peaks (Figure 6a). These peaks correspond to the energies of the ideal crystalline structure, which are also shown for reference. On the other hand, when both types of disorder are present, DOS has a wider distribution of energies (Figure 6d).

We will consider the states with a value of localization length  $L$  less than 15, as localized states because all the states within first 0.2 eV from the top of the valence band have  $L$  smaller than 15 (see Figure 6e). In the structures with disordered side chains, most of the states are delocalized (Figure 6b). When both main and side chains are disordered, both localized and delocalized states exist (Figure 6e) but all states are localized in the spectral region of 0.2 eV below the highest state. Qualitatively similar results were obtained in amorphous P3HT<sup>[55]</sup> and from other calculations in ordered polymers.<sup>[53,61]</sup> From the comparison of the results for the structure with disorder in side chains only and the structure with disorder in both main and side chains, one can conclude that disorder in main chains is mainly responsible for the localization of charge carriers in ordered P3HT.

Charge transport in ordered polymers takes place along the main chain and the  $\pi$ - $\pi$  stacking direction. Therefore, the localization length in the  $\pi$ - $\pi$  stacking direction is also of particular interest. It can be considered as the number of different chains that a state is localized on. Localization length in the  $\pi$ - $\pi$  stacking direction  $L_b$  was calculated using a similar formula as for the total localization length, with a redefinition of the expansion coefficients in such a manner that they refer to chains, instead of fragments. The energy dependence of  $L_b$  is qualitatively similar as the energy dependence of  $L$  (Figure 6c,f). In the case when both types of disorder are

present, the highest states in the valence band have the values of  $L_b$  around 2. These states are predominantly localized on two neighboring chains due to significantly high electronic coupling between the chains. The wave function of the HOMO state in that case is shown in **Figure 7b**. On the other hand, when the disorder in side chains only is present, the wave functions are delocalized among a larger number of chains, as can be seen from Figure 6c and from the wave function of HOMO state shown in Figure 7a.

With the presented results, one can build a detailed picture on the role that the constituents of the polymer material have when the effects of thermal disorder are concerned. Side chains create a disordered electrostatic potential which leads to some degree of localization in the  $\pi$ - $\pi$  stacking direction. Although these chains are flexible and have a rather disordered shape, their effect is not very strong because charge transfer between C and H atoms is small and therefore the electrical dipoles that create the electrostatic potential are weak. The dominant cause of localization then comes from disorder in the shape of main chains which has a strong effect both on the intrachain and interchain electronic coupling. Interestingly, the interchain electronic coupling remains sufficiently strong to delocalize the carrier over two chains.

Other simulations of thermally disordered polymers also lead to the results that are consistent with parts of this picture. It was demonstrated elsewhere<sup>[61]</sup> that electronic states on a single polythiophene main chain, in the absence of side chains exhibit localization. The localization of the states on a single chain of the PBTTP polymer lamella (where side chains were not included in the calculation) was predicted from calculations in the literature.<sup>[53]</sup>

The importance of thermal disorder in small molecule based organic crystals is now well appreciated<sup>[33]</sup> and will be only briefly discussed here. Its effects have been mostly studied within an one dimensional model where electronic coupling between the molecules  $n$  and  $n+1$  depends on the displacements of these molecules  $u_n$  and  $u_{n+1}$  as  $t(u) = t[1 + \alpha(u_{n+1} - u_n)]$ .<sup>[33,62,63]</sup> In Figure 1b,c (top panel) we present the DOS and the localization length for such a system consisting of 100 sites, obtained by averaging over 25 000 realizations of the system, with atomic displacements from the Gaussian distribution with standard

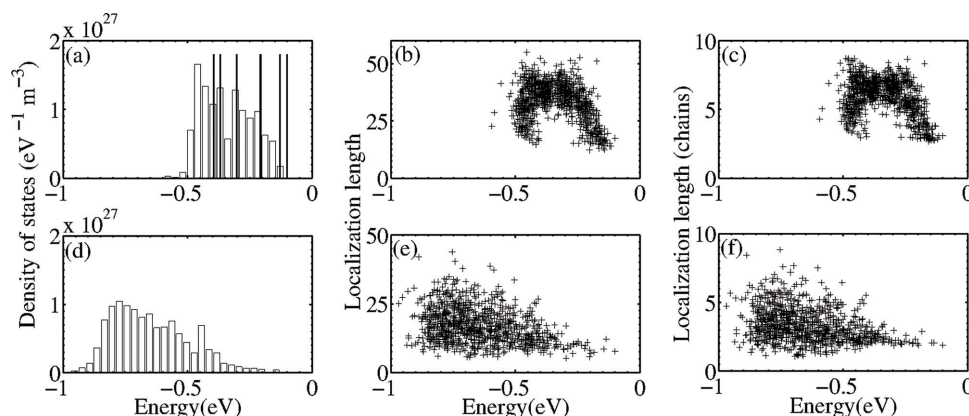


**Figure 6.** DOS for a) structures with disorder in side chains only and d) structures with disorder in both main and side chains; total localization length for b) structures with disorder in side chains only and e) structures with disorder in both main and side chains; localization length in the  $\pi$ - $\pi$  stacking direction for c) structures with disorder in side chains only and f) structures with disorder in both main and side chains.

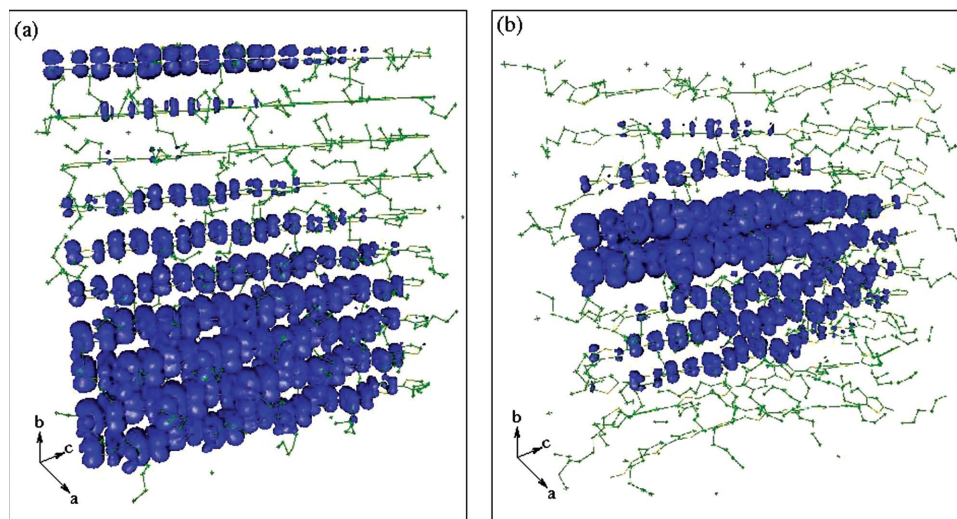


**Figure 7.** Isosurfaces of wave function moduli squared for HOMO state of P3HT with a) disorder in side chains only and b) disorder in both main and side chains. Isosurfaces correspond to the probability of finding a hole inside the surface of 90%.

deviation  $\sigma = \sqrt{\frac{2\lambda k_B T}{t\alpha^2}}$ , where  $T$  is the temperature and  $\lambda = 0.1$ . As can be seen from the figure, the presence of localized states near the band edge is a feature of this class of systems, while the states further away from the band edge are less localized. The increase of temperature leads to a wider tail in the DOS (see top part of Figure 1b) and to better localization of the states away from the band edge (see top part of Figure 1c). In the calculations performed starting from realistic atomic structure from MD snapshots and using the CPM and OFM to perform electronic structure calculations the presence of localized states at the band edge is also obtained.<sup>[38,64]</sup>

#### 4.3. Grain Boundaries in Polycrystalline Organic Semiconductors Based on Small Molecules

Organic thin films based on small molecules are typically polycrystalline. It implies that they contain grain boundaries which separate the grains with different crystalline orientations. Grain boundaries are considered to be the most limiting intrinsic factor for charge carrier transport.<sup>[18,20,21,65–67]</sup> Nevertheless, the precise way in which they affect the electronic properties is not well understood. Quite a few works suggest the presence of trap centers at the boundaries,<sup>[18,19,21,65,68–71]</sup> The trapping of carriers at these centers leads to the drop in charge carrier mobility. On the other hand, there are suggestions that grain boundaries

act as barriers for charge carriers, which inhibit the transport across the boundary.<sup>[72,73]</sup> Therefore, detailed electronic structure calculations are required to gain better understanding of the effect of grain boundaries.<sup>[71]</sup>

Initial atomic structure used in the simulation consists of two joined naphthalene crystalline grains with different crystalline orientations. Low-angle grain boundaries (misorientation angles from 5° to 20°) are most relevant since the calculations indicate that the energy of the structure increases as the angle of misorientation between the grains increases. Structures were optimized using MC simulations. Simulations are firstly performed at a finite temperature of 300 K and subsequently cooled down to 0 K, in order to exclude thermal disorder effects, which can additionally affect the electronic structure, as discussed in Section 4.2. Electronic structure calculations were performed using the CPM and the FSM. Since the electronic transport in such materials is two-dimensional, calculations were performed for single layers of polycrystalline naphthalene, each containing around 1400 atoms.

Wave functions of the electronic states at the top of the valence band for the system consisting of two crystalline grains with a misorientation angle of 10° are shown in **Figure 8**. By inspecting the isosurfaces for the presented states, one can notice three types of states: 1) states localized on two molecules at the boundary (Figure 8a); 2) other states localized at the boundary (Figure 8b), and 3) delocalized states (Figure 8c).

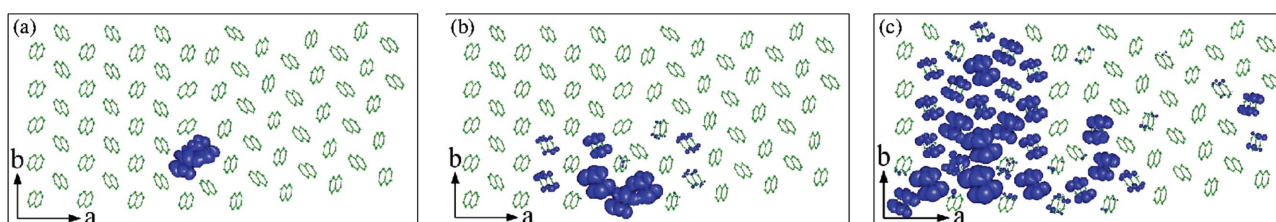


**Figure 8.** Isosurfaces of wave function moduli squared of the a) HOMO, b) HOMO-3, and c) HOMO-9 state of naphthalene grain boundary with misorientation angle of 10°. Isosurfaces correspond to the probability of finding a hole inside the surface of 90%.

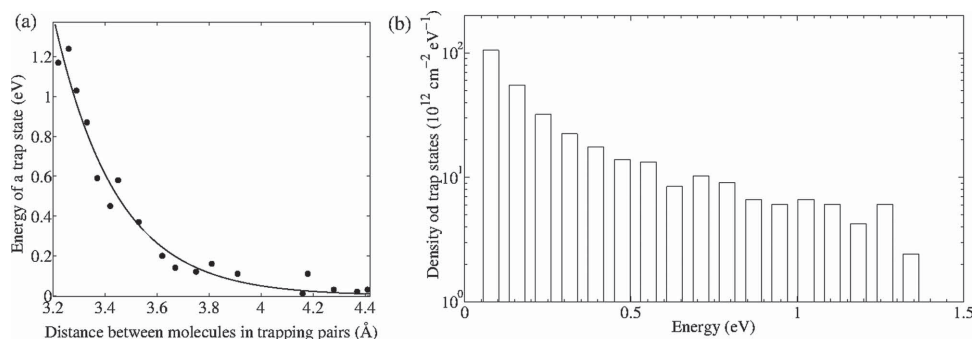


**Figure 9.** a) The dependence of the energy of trap states at the grain boundary on the distance between molecules which form the traps. The data obtained from all simulated systems are presented in the figure. Energies of the trapping states are defined with the top of the valence band as a reference level. b) Density of trap states for the system of two naphthalene crystalline grains with misorientation angle of  $10^\circ$ .

Results for other simulated systems are qualitatively the same. The highest states are always localized on molecule pairs at the boundary. Molecules in such pairs have mutual distance significantly smaller than the distance between neighboring molecules in a crystal. States created by these pairs can be very deep in the band gap, even more than 1 eV above the band edge. It is well-known that the decrease in the distance between the molecules increases the electronic coupling between them.<sup>[74]</sup> Therefore, higher electronic coupling between molecules at the boundary is responsible for the creation of the trap states in the band gap. Other localized states produce shallow traps, with the depth of up to 0.1 eV. Delocalized states start to appear at certain energy where the energy spectrum becomes continuous. Such states exist in a single crystal and they are not induced by a boundary. However, our results indicate that delocalized states are mostly localized at one side of the boundary (as in Figure 8c). For such states, grain boundary acts as a barrier.

Simulation results indicate that the energy of a trap state is strongly correlated to the distance between molecules which form the trap, as shown in **Figure 9a**. The exponentially decreasing function gives the best fit to this dependence. Additionally, the changes in the distances between molecules in trap centers after the atomic relaxation in MC simulation are not larger than 0.1 Å. Therefore, one can predict the energy of a trap state without MC simulations and electronic structure calculations, only by using the distance between the molecules and the fitting function. This method produces an error of around 0.1 eV. Using this approach, the density of trap states for large grain boundaries can be calculated. In **Figure 9b** the density of trap states for large grain boundary (around 30 nm) with misorientation angle of  $10^\circ$  is given.

The features obtained from a detailed atomistic simulation can largely be understood from a simple model of a grain boundary. We consider a special case of the model given by Equation 1–3 where the system consists of 100 sites arranged on a line. Electronic coupling between neighboring sites is  $t$ , except for the coupling between the two middle sites which is given by a uniform random number between 0 and  $2t$ . Different electronic coupling between the middle sites models the effect of the grain boundary on electronic properties. In **Figure 1b,c** (middle panel) the DOS and the dependence of the localization length on energy obtained by averaging the results over 25 000 different realizations of the system are presented. The presence

of localized states within the band gap of the material induced by the grain boundary is evident from the figures.

## 5. Electronic Transport

### 5.1. Amorphous Polymers

Understanding the relationship between the atomic structure of the material and its electrical properties is a highly challenging task. This is the case in particular for disordered polymers where there is no periodicity of the atomic structure that can be exploited. The details of the atomic structure are also not very well known. In addition, specialized and efficient methods are required to perform electronic structure calculations on large supercells that are needed to extract sufficient statistics about the electronic properties of disordered materials.

For these reasons, phenomenological approaches were typically used to model electrical transport in disordered organic materials. In these approaches, one assumes that the system consists of a set of sites, characterized by their energy and the spatial position. Charge carrier transport in such a system then takes place by hopping between these sites. The energies of sites are drawn from a predefined distribution such as the Gaussian or the exponential distribution. The most usual assumptions about the spatial positions of sites are that they are located on cubic lattice or that they are distributed randomly in space with a uniform distribution. The probability of carrier hopping from site  $i$  to an unoccupied site  $j$  in a unit of time is often assumed to take the Miller-Abrahams form  $W_{ij} = W_0 \exp(-2R_{ij}/a)$  for downward transitions ( $E_i \geq E_j$ ) and  $W_{ji} = W_0 \exp[-(E_i - E_j)/(k_B T)]$  for upward transitions ( $E_i < E_j$ ). In previous equations,  $R_{ij}$  is the spatial distance between sites  $i$  and  $j$ ,  $E_i$  is the energy of the carrier at site  $i$ ,  $T$  is the temperature, while  $W_0$  and  $a$  are constant coefficients in the exponentially decaying dependence of  $W_{ij}$  on  $R_{ij}$ . Such a model of electronic transport in disordered materials (when Gaussian DOS is assumed) is usually referred to as the “Gaussian disorder model”.<sup>[75–78]</sup>

Due to the simplicity of the phenomenological approaches, these have become quite popular and they are often used to fit the experimental data, such as the dependence of mobility on temperature. Nevertheless, the shortcomings of these models

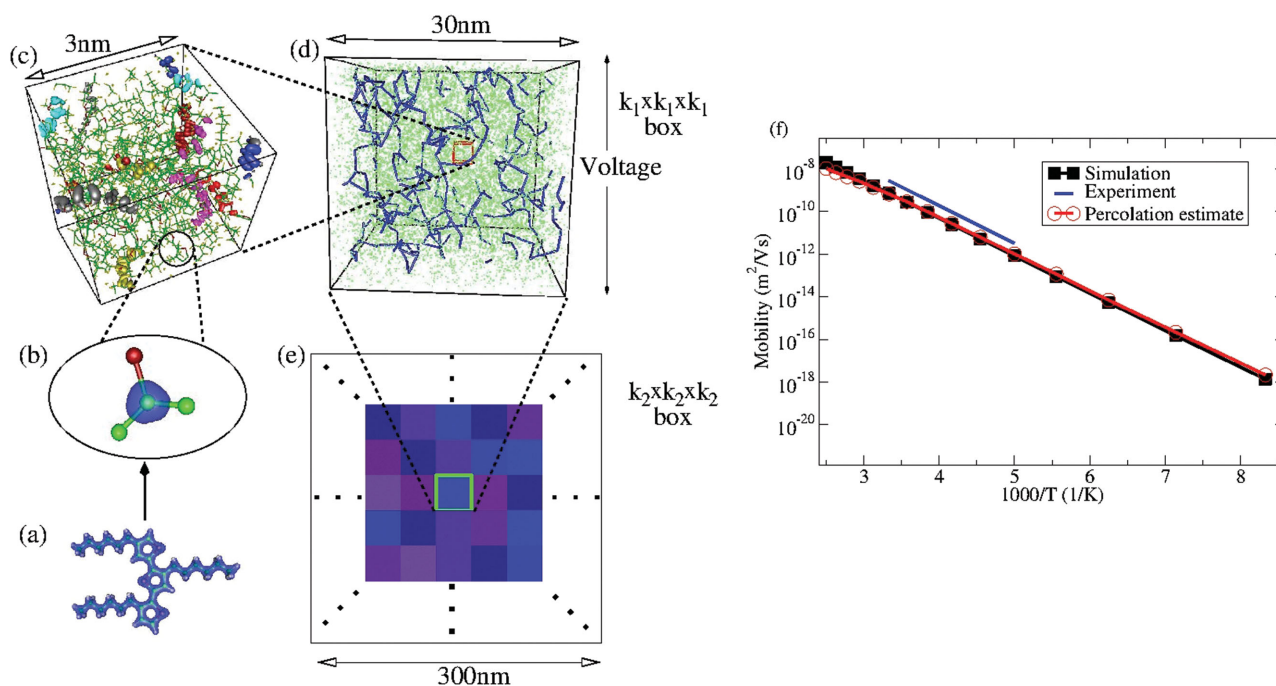


**Figure 10.** Schematic representation of the multiscale procedure for simulation of charge transport in amorphous polymers: a) Atomic structure and electronic charge density of the small molecule used to generate the charge density motifs; b) Charge density motif assigned to one atom type in the system; c) The atomic structure and valence band wave function isosurface plots of the disordered polymer; d) Transport sites (green dots) and the relevant current paths through the material (blue lines) when the voltage is applied in the direction indicated; e) Continuum system at the final length scale; f) Temperature dependence of hole mobility in P3HT polymer obtained from the described procedure (squares), its comparison to experimental data from the literature<sup>[87,88]</sup> (solid line) and the estimate from percolation theory (circles).

are the lack of clear physical meaning of the concepts and parameters of the model and the lack of their relation to atomic structure of the material. For example, is not clear what the “sites” in the model correspond to in the real physical system. If it is assumed that the sites are distributed on a cubic lattice, it is questionable how to choose the lattice constant. Miller-Abrahams form for the transition rates was derived originally in the context of carrier hopping between impurities in solids.<sup>[79]</sup> If the wave function of a carrier on the impurity is spherical, then the overlap between the wave functions on the two impurities decays exponentially with the distance between the impurities and the assumption of Miller-Abrahams form is quite plausible. On the other hand, as seen in Figure 3a, the wave functions in disordered polymers have a quite different, elongated shape, and it is questionable if such an expression is applicable to them.

Due to mentioned shortcomings of phenomenological models, the development of an approach that would link the atomic structure of the material to its electrical properties is of great interest. We have developed such an approach that links the quantities on four length scales to obtain the macroscopically measurable property of the material, such as the charge carrier mobility.<sup>[30]</sup> The whole approach in its present form focuses on homogeneous strongly disordered materials. Presently, it cannot be directly applied to more complex materials that contain both disordered and ordered phases. Nevertheless, the parts of the approach and the ideas from the approach will certainly be helpful in the development of the approach for treatment of more complex materials.

At the smallest length scale (on the order of few angstroms), we perform DFT calculations on small molecules (shown in Figure 10a) to obtain the motifs used in the CPM (shown in Figure 10b).

At the next length scale (Figure 10c), we perform electronic structure calculations to obtain the energies and wave functions of charge carriers. The atomic structure of the polymer material at this length scale is obtained from classical MD using a simulated annealing procedure, as described in Section 3. Electronic structure calculations at this length scale are performed using the CPM which constructs the single particle Hamiltonian, which is then diagonalized either using the FSM or the OFM. At this length scale, we also calculate the charge carrier hopping rates between the states as

$$W_{ij} = \pi \sum_{\alpha} \frac{|M_{ij,\alpha}|^2}{\omega_{\alpha}} \left[ (N_{\alpha} + 1) \delta(E_i - E_j - \hbar\omega_{\alpha}) + N_{\alpha} \delta(E_i - E_j + \hbar\omega_{\alpha}) \right] \quad (6)$$

where  $W_{ij}$  is the probability of hopping from state  $i$  to state  $j$  in a unit of time,  $E_j$  and  $E_i$  are the energies of states,  $\hbar\omega_{\alpha}$  is the energy of phonon of mode  $\alpha$ ,  $N_{\alpha}$  the number of phonons in that mode given by the Bose-Einstein distribution,  $M_{ij,\alpha}$  and is the electron-phonon coupling constant between electronic states  $i$  and  $j$  due to phonon mode  $\alpha$ . The phonon modes are obtained from the same classical force field that was used in MD simulations by diagonalizing the corresponding dynamical matrix. The electron-phonon coupling constants are obtained

from the CPM by calculating the change in the single particle Hamiltonian due to displacements according to a given phonon mode.

One should pay particular attention to the size of the simulation box at this length scale. It is absolutely necessary that it is larger than the localization length of strongly localized wave functions (otherwise the obtained wave functions would not be representative of wave functions in real system). On the other hand, its size is limited by the computational cost of electronic structure calculations. With the combination of CPM and OFM, we can calculate the system that contains on the order of 10 000 atoms which corresponds to box size on the order of 5 nm. Such a size is sufficient to obtain reliable wave functions. Nevertheless, with such a calculation we obtain several tens of wave functions in the spectral region within  $\approx 0.5$  eV, which is the spectral region of interest for electrical transport properties. This is too little states for the extraction of macroscopic parameter of the material such as the charge carrier mobility because a different random realization of the system would lead to a completely different mobility. For this reason, we need to go to the next length scale to simulate charge carrier transport. To get sufficient information to construct the system on the next length scale, we repeat the calculation on this length scale many times for different random realizations of the system.

At the next length scale, we consider the system as a set of sites among which the charge carriers are hopping [shown in Figure 10d]. The simulation box is constructed by putting together  $k_1 \times k_1 \times k_1$  (typically  $k_1 = 10$ ) small boxes whose size is equal to the size of the box on the previous length scale. The positions and energies of the sites in each of the small boxes are taken from the simulation on the previous length scale, by randomly choosing one of the realizations of the system on the previous length scale and randomly rotating it in space. It is well known<sup>[86]</sup> that the conductance at low electric fields for hopping transport is equal to the conductance of a network of resistors constructed by connecting sites  $i$  and  $j$  with a resistor of conductance  $G_{ij} = \frac{e^2}{k_B T} n_i W_{ij} = \frac{e^2}{k_B T} n_j W_{ji}$ , where  $n_i$  is the occupation of site  $i$ . The hopping rates between the sites from the same small box are directly available from the simulation on the previous length scale, while the hopping rates between different boxes are approximated in a manner that retains their statistical averages.<sup>[30]</sup> The calculations for different realizations of the system at this length scale (where the simulation box size is typically on the order of 20–30 nm) still yield different mobilities, which vary within one to two orders of magnitude depending on temperature.

To obtain the final mobility representative of the mobility of bulk amorphous polymers, we therefore need to go one length scale further (shown in Figure 10e). At this final length scale, we consider the system as the continuum with spatially varying conductivity. The simulation box is again constructed by putting together  $k_2 \times k_2 \times k_2$  (with typical  $k_2 = 10$ ) small boxes whose size is equal to the box size on the previous length scale. Each of these boxes is considered as a uniform but anisotropic conductor whose conductivity is determined from the result on the previous length scale. The mobility in direction  $d$  (where  $d = x, y$  or  $z$ ) is calculated as  $\mu_d = G_d / (enL)$ , where  $G_d$  is equivalent

conductance in direction  $d$ ,  $n$  is the concentration of carriers, and  $L$  is the box size dimension at this length scale. We will present the results for the limit of low carrier concentration, when  $G_d$  is proportional to  $n$  and the mobility is independent of carrier concentration. At this length scale (with the box size on the order of 300 nm), one finally obtains the mobility which is nearly independent on random realization of the system. It is interesting to note that a very similar result for the mobility would be obtained if one simply took the geometrical average of the mobilities obtained at the previous length scale instead of performing the simulation of the continuum system at this length scale.

Our approach overcame the issue of insufficiently large size of the box used in electronic structure calculations through the construction of larger system on the next length scale from the information obtained on previous length scale. At each length scale we check if the simulation box is big enough by repeating the calculation on that length scale for different random realizations of the system. If the conductance obtained for different realizations significantly varies, this gives an indication that the system is not large enough and that one needs to go one length scale further. The information gained from repeated calculations is then used to construct the system on the next length scale. At the final scale the variations of the conductance for different realizations of the system are small which indicates that the simulation box on that length scale is large enough. An interesting alternative to our approach was discussed in another study.<sup>[80]</sup> That approach is based on the fact that at higher temperatures the carriers visit a significantly larger number of sites during the transport and for that reason smaller system size is required to obtain the mobility at higher temperatures than at low temperatures. One can then calculate the mobility of the small system at high temperature and use it to extrapolate to the mobility of bulk at low temperatures as described elsewhere.<sup>[80]</sup>

Temperature dependence of the mobility of amorphous P3HT polymer is presented in Figure 10f. We find that the mobility is thermally activated and its temperature dependence fits well the expression  $\mu(T) = \mu_0 \exp[-E_A / (k_B T)]$ , with activation energy of  $E_A = 347$  meV and the mobility at room temperature of  $\mu(T = 300\text{K}) = 0.71 \times 10^{-9} \text{ m}^2 \text{ V}^{-1} \text{ s}^{-1}$ . On the other hand, experimental results<sup>[87,88]</sup> yield  $E_A = 350$  meV and  $\mu(T = 300\text{K}) = 2.8 \times 10^{-9} \text{ m}^2 \text{ V}^{-1} \text{ s}^{-1}$ . Therefore, the simulation results are in quite good agreement with experiment since the correct value of activation energy is obtained and the correct order of magnitude of the mobility.

The fact that we needed to perform the simulation at several length scales up to the scale of hundreds of nanometers is a direct consequence of disordered nature of the system. For a disordered system the length scale beyond which the system starts behaving as bulk is much larger than for ordered systems. The fact that we needed to extend our simulation to the 100 nm length scale indicates that this is exactly the length scale beyond which the portion of the disordered polymer material behaves as bulk when electrical transport characteristics are concerned. All devices of smaller size would exhibit different characteristics for different realizations of the device.

In ordered materials, current is uniformly distributed through the material (at the length scale beyond the

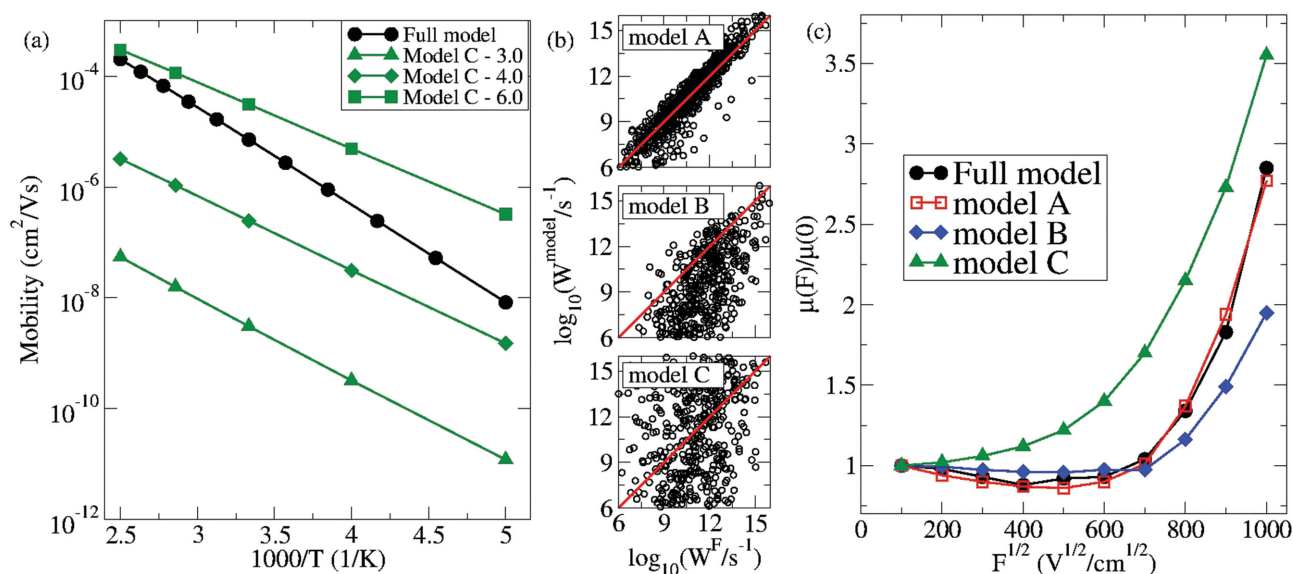


**Figure 11.** a) Temperature dependence of the mobility in the full model and using the model with Miller-Abrahams rates (model C). The value of the parameter  $a$  (in Angstroms) in model C is indicated in the legend. b) The comparison of hopping rates in different models with the ones obtained in the full model. c) Electric field dependence of the mobility at room temperature within different models. The parameters of the models A–C were chosen to fit the temperature dependence of the mobility from the full model.

interatomic distances). On the other hand, this is not the case in disordered materials and it is very interesting to inspect the current paths in the material. These are presented in Figure 10d. In the figure, the sites where the current is larger than 5% of the maximal current in the system are connected with lines. The currents between these sites contribute to at least 75% of the total current at each cross section perpendicular to the direction of the applied voltage. For these reasons the current paths shown in the figure can be considered as relevant current paths in the material. From visual inspection of the figure, one can notice that the overall current flow is determined by a relatively small number of current paths, which gives an indication that percolation theory might be appropriate for the description of current flow in the system.

Percolation theory often gives a good description of transport properties in disordered systems. In the context of our system, modeled as a conductor network, percolation theory suggests that the current paths are formed at the place where a continuous network of connections that spans the whole system can be formed, where connections are formed between each two sites with a conductance larger than some critical conductance  $G_c$ . The criterion that can be used to check if the continuous network that spans the system was formed is that the number of connections per site is larger than some critical value  $a_c$ . We find that the conductivity of the material can reliably be estimated (see Figure 10f) from percolation theory as  $\sigma = G_c / L_c$ , where  $G_c$  was determined from  $a_c = 3.2$  and  $L_c$  is taken to be equal to characteristic distance between the sites  $L_c = 1.5$  nm. Further confirmation of the appropriateness of the percolation theory comes from the fact that all resistors in the relevant current path indeed have  $G_c > G_c$ .

In our approach, we calculate the transition rates between the states using a rather detailed formula given by Equation 6 which includes the coupling to all phonon modes. To calculate

these rates, one needs to calculate the wave functions, the phonon modes, and the electron-phonon coupling constants, which is computationally very demanding. On the other hand, widely used Miller-Abrahams expression contains only the energies of electronic states and the distance between the sites. It is therefore of great interest to determine to what extent can the full expression for transition rates (Equation 6) be simplified. Such an insight would be helpful to reduce the computational cost of the described multiscale procedure. Moreover, this insight will help us to address an important question about the main physical quantities that determine the charge carrier mobility. While it is widely understood that the mobility is strongly dependent on electronic DOS, one can imagine that the phonon DOS, the details of wave functions overlaps, as well as the details of the phonon modes could be important as well.

The hopping rates in the system, calculated using Equation 6 that takes into account the interaction with all phonon modes largely deviate from the traditional Miller-Abrahams form (bottom panel in Figure 11b). The main reason for this deviation is that the wave functions have a strongly anisotropic shape and therefore their overlap does not simply decay exponentially with distance between them.

Next, we would like to understand the consequences of the differences between the rates obtained using Miller-Abrahams form and the full model on electrical transport. The comparison of the mobilities, shown in Figure 11a, indicates that for a physically realistic prefactor  $W_0 = 10^{14}$  s<sup>-1</sup>, regardless of the values of the parameter  $a$ , the slope of the dependence is different. Therefore, the model with Miller-Abrahams hopping rates cannot reproduce the results of the detailed model, regardless of the choice of parameters, as long as they are physically realistic. We find that the dependence can be reproduced only with physically unrealistic pair of parameters  $W_0 = 6.3 \times 10^{20}$  s<sup>-1</sup> and  $a = 2$  Å.

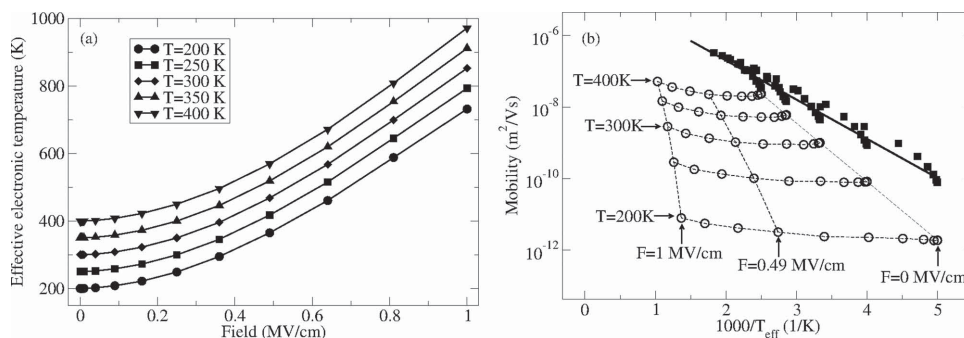


**Figure 12.** a) Dependence of effective electronic temperature on electric field for different values of lattice temperature. b) Dependence of mobility on effective electronic temperature in full model (circles) and in model C with  $a = 6 \text{ \AA}$  (squares).

While we have shown that the model with Miller-Abrahams rates yields quantitatively significantly different results than the full model, we demonstrate another example where the model with Miller-Abrahams rates gives even a qualitatively different result. This result concerns the importance of the concept of effective electronic temperature for the system in a finite electric field. The effective electronic temperature is defined from the fit of charge carrier distribution to a Boltzmann distribution and its dependence on electric field for several lattice temperatures is shown in **Figure 12a**. An important question about the effective electronic temperature is whether it can be used to replace the joint effect of electric field and lattice temperature. If this is the case, then the dependence of mobility on electronic temperature falls into one curve. As seen from **Figure 12b** we reproduce the results of earlier studies that this is the case in the model with Miller-Abrahams rates,<sup>[81,82]</sup> while we find that this is not the case in the full model.<sup>[83]</sup> Consequently, the model with Miller-Abrahams rates yields a qualitatively different conclusion related to the importance of effective electronic temperature than a realistic model.

Having established that the model with Miller-Abrahams rates can yield the results which are both qualitatively and quantitatively different, we would like still to find a model which is simpler than our detailed model, and yet accurate enough. We therefore introduce several approximations to the hopping rate expression. In first approximation we assume that the electron-phonon coupling constant is simply proportional to the overlap of the wave function moduli  $S_{ij} = \int d^3 \mathbf{r} |\psi_i(\mathbf{r})| |\psi_j(\mathbf{r})|$ , which then yields the model that we call model A where the downward hopping rate is given by the expression

$$W_{ij}^A = \beta^2 S_{ij}^2 [N(E_{ij}) + 1] D_{\text{ph}}(E_{ij}) / E_{ij} \quad (7)$$

where  $\beta$  is the proportionality factor between electron-phonon coupling constants and wave function moduli overlaps,  $D_{\text{ph}}(E_{ij})$  is the phonon DOS normalized to satisfy  $\int_{-\infty}^{\infty} dE D_{\text{ph}}(E) = 1$  and  $E_{ij} = |E_i - E_j|$ . Further simplification can be made by assuming that the wave function overlap decays exponentially with distance which yields model B where the downward hopping rate is given as

$$W_{ij}^B = \beta^2 \exp(-2R_{ij}/a) [N(E_{ij}) + 1] D_{\text{ph}}(E_{ij}) / E_{ij} \quad (8)$$

Finally, if all the energy dependence is ignored in the last expression, one gets the model C which is the Miller-Abrahams

expression. The free parameters in all these models can be adjusted to fit the temperature dependence of the mobility in the limit of low carrier concentration (albeit sometimes with physically unrealistic set of parameters), but the question is whether they can then be used to predict other properties. One of these properties is the electric field dependence of the mobility in the limit of low carrier concentration. We find that only model A can reproduce the mobility from the full model, see **Figure 11c**. The microscopic origin of this lies in the fact that hopping rates in model A still quite decently reproduce the hopping rates from the full model, which is not the case for models B and C, see **Figure 11b**.

We also note in passing that the mobility generally increases with an increase in electric field (**Figure 11c**), while for models A and C it exhibits a slight decrease with increasing field at low electric fields (negative differential conductance). It has been argued<sup>[77,84,85]</sup> that negative differential conductance obtained in some experiments and simulations is an artefact of the time-of-flight and kinetic Monte Carlo mobility extraction procedure which ignores the presence of diffusion current. Due to only slight negative differential conductance obtained in our simulation, it is difficult to establish with certainty if negative differential conductance is present or not.

Having established that the model A captures the most important features of the hopping rates, we can identify what are the physical quantities that determine the transport. In addition to electronic DOS, the phonon DOS is important since it appears explicitly in our model for hopping rates. Details of the wave function overlaps are important as well. On the other hand, the fact that we could simplify our initial expression to this model implies that the details of the phonon modes are not of primary importance.

Therefore, these results suggest that in addition to the widely appreciated fact that electronic DOS is important for electrical transport, the wave function overlap and the phonon DOS are also of importance.

## 5.2. Other Organic Semiconductors

There is a consensus that charge transport in amorphous polymers takes place by hopping between the states localized due to static disorder present in the material. On the other

hand, thermal disorder present in ordered organic materials is of dynamic nature and its influence on electrical transport properties is less transparent. This is probably one of the main reasons why a consensus about the mechanism and nature of charge transport in ordered organic materials has not been reached yet. In this subsection, we will discuss the results obtained in previous sections in view of their consequences for electrical transport properties.

### 5.2.1. Small Molecule Based Organic Crystals

Electrical transport in small molecule based organic crystals has been modeled using a variety of approaches. A popular approach due to its relative simplicity is based on Marcus theory of charge transfer.<sup>[31]</sup> In such an approach, the crystal is considered as a set of molecules and charge transfer rates between any two molecules are evaluated from semiclassical Marcus theory or its generalizations. The mobility through the material is then calculated from Master equation or kinetic Monte Carlo approach. However, one should be careful regarding the limitations of this approach.<sup>[37,89]</sup> Such a methodology ignores coherent propagation of the carrier between the molecules and it assumes that electronic coupling between the molecules is just a perturbation. As a result, it gives thermally activated dependence of mobility on temperature, which is in contrast to experimental results from the literature.

Other set of approaches<sup>[90–92]</sup> is based on the canonical transformation of the Hamiltonian to a new basis where electron-phonon interaction acts just as a perturbation. These approaches can yield the mobility that decreases with an increase of temperature. However, due to the approximations used in the formalism (including often neglecting of non-local electron-phonon coupling), the reliability of these approaches is still the subject of investigation.

As pointed out in Section 4.2, the eigenstates of the Hamiltonian obtained by freezing the atomic coordinates at a certain moment of time (so called adiabatic states) exhibit localization. However, as the time evolves the Hamiltonian changes and it is not clear whether the carrier will remain in the new adiabatic state or make a transition to some other state. An approach that transparently takes into account the dynamic localization of carriers combines classical MD with time propagation of the Schrodinger equation according to the Hamiltonian that depends on atomic coordinates obtained from MD.<sup>[33,93]</sup> This approach is referred to as Ehrenfest dynamics. In simulations based on Ehrenfest dynamics,<sup>[33]</sup> experimentally observed trend of mobility that decreases with increasing temperature was obtained. Given the presence of localization of band edge states (and delocalization of states further away from the band edge), this trend is something that may not be expected since higher temperature should promote the carriers from localized to delocalized states and improve the transport. However, one should note that the spectral region with localized carriers is rather narrow (smaller than  $k_B T$  at room temperature, see Figure 1b,c, top parts) and that even a relatively small temperature is sufficient to promote the carriers to delocalized states. Therefore the temperature dependence of the mobility is likely determined by other effects, such

as the decrease of the localization lengths with an increase of temperature. One should also note that Ehrenfest dynamics is known to suffer from the issue that the mean energy of carriers is substantially larger than the correct one,<sup>[38,94]</sup> Fewest switches surfaces hopping method is a modification of Ehrenfest dynamics that solves this issue.<sup>[95]</sup> In simulations based on this approach<sup>[38]</sup> with the Hamiltonian obtained from CPM, it was found that the transition from one adiabatic state to another takes place when the two adiabatic states cross each other and that these transitions dominantly determine the carrier transport. Another issue with approaches based on the combination of classical MD for the motion of nuclei and quantum evolution of electronic degrees of freedom is that the phonons are treated classically, which is an approximation whose validity has yet to be investigated. The range of validity of surface hopping approaches (in particular for high mobility materials with band like transport) also remains a topic for further investigation.<sup>[96]</sup>

### 5.2.2. Grain Boundaries in Small Molecule-Based Organic Crystals

Results for electronic structure of polycrystalline naphthalene, presented in Section 4.3, unambiguously confirm the presence of trap centers at the grain boundary. From the calculations, we have estimated that the number of trap states per unit of volume (assuming the size of the grains is  $1\ \mu\text{m}$ ) is  $N_t = 9 \times 10^{17}\ \text{cm}^{-3}$ , while the number of states in the valence band in naphthalene bulk is  $N_v = 6.1 \times 10^{21}\ \text{cm}^{-3}$ . These estimates are in good agreement with previously reported results for density of trap states in similar materials.<sup>[18,65]</sup>

Since  $N_t$  is relatively significant in comparison to  $N_v$ , traps induced by grain boundaries are expected to have a significant affect on electronic transport, especially in devices which operate in low carrier density regime, such as light-emitting diodes and solar cells. In devices which operate in high carrier density regime, such as field-effect transistors, carriers fill the traps, which affects the transport only through electrostatic barriers created by trapped carriers.<sup>[66,68,69]</sup>

A detailed model of electrical transport at a single grain boundary has not yet been developed. One of the reasons for that is the lack of complete understanding of transport model in bulk crystals, which should certainly be an ingredient of the single grain boundary transport model. Since, as discussed in Section 4.3, the grain boundary acts somewhere as a trap, and somewhere as a barrier, the current flow through the boundary will be spatially nonuniform and one may expect that it contains very interesting physics.

### 5.2.3. Ordered Polymers

As shown in Section 4.2, in ordered polymers there is a spectral region within first 0.2 eV from the top of the valence band where only localized states exist. These states were found to be persistently localized in the sense that their position does not significantly vary during nanosecond timescales.<sup>[61]</sup> Previous results,<sup>[61]</sup> as well as our calculations, show that localization length does not vary significantly with temperature in the range from 100K to 300K. On the other hand, temperature increase

supports hopping from localized to delocalized states.<sup>[97]</sup> Therefore, the promotion of carriers from localized to delocalized states in ordered polymers could be the reason for thermally activated transport, which was observed in such systems in mobility measurements.<sup>[98]</sup>

At this point, it is interesting to discuss the difference in the temperature dependence of the mobility observed in small molecule based organic crystals and ordered polymers. Both classes of systems exhibit a spectral region near the band edge where only localized states exist, which is followed by the region with more delocalized states. However, this spectral region is much wider in polymers, while it is so narrow in small molecule based crystals that a large number of carriers is present in delocalized states even at relatively small temperatures. On the other hand, in polymers significant activation energy is required to promote the carriers to delocalized states, which may lead to thermally activated transport.

## 6. Conclusion

With the help of atomistic simulations, one can currently get important insights into the wave function localization lengths and the electronic DOS for a variety of organic semiconductor structures, such as amorphous polymers, ordered polymer regions, small molecule based organic crystals and grain boundaries in organic crystals. In the case of amorphous polymers, which exhibit strong static disorder, these results can be directly used in combination with a multiscale approach to evaluate measurable macroscopic material properties, such as the charge carrier mobility. Atomistic multiscale simulations are then necessary to obtain quantitatively correct results, while in some cases even qualitatively correct results cannot be obtained without the use of such detailed simulations. In other organic semiconducting materials and structures, where the effects of dynamic disorder are of significant importance, the results of atomistic simulations give some indication about the nature of charge carrier transport. Further research is certainly needed to better understand the carrier transport mechanism in these materials which will presumably also lead to the development of methods for a better quantitative description of electrical transport. Moreover, simulation approaches described in this article certainly open the way to study complex structures exhibited in realistic organic materials—such as the interfaces between ordered and disordered regions in conjugated polymer based materials.

## Acknowledgements

This work was supported by a European Community FP7 Marie Curie Career Integration Grant (ELECTROMAT), the Serbian Ministry of Education, Science and Technological Development (Project ON171017) and FP7 projects PRACE-3IP and EGI-InSPIRE.

Received: July 21, 2014

Revised: August 22, 2014

Published online: September 22, 2014

- [1] H. E. Katz, J. Huang, *Ann. Rev. Mater. Res.* **2009**, *39*, 71–92.
- [2] T. Ameri, P. Khoram, J. Min, C. J. Brabec, *Adv. Mater.* **2013**, *25*, 4245–4266.
- [3] K.-J. Baeg, M. Binda, D. Natali, M. Caironi, Y.-Y. Noh, *Adv. Mater.* **2013**, *25*, 4267–4295.
- [4] H. Dong, H. Zhu, Q. Meng, X. Gong, W. Hu, *Chem. Soc. Rev.* **2012**, *41*, 1754–1808.
- [5] Y. Lin, Y. Li, X. Zhan, *Chem. Soc. Rev.* **2012**, *41*, 4245–4272.
- [6] D. Briand, A. Oprea, J. Courbat, N. Barsan, *Mater. Today* **2011**, *14*, 416–423.
- [7] M. D. Angione, R. Pilolli, S. Cotrone, M. Magliulo, A. Mallardi, G. Palazzo, L. Sabbatini, D. Fine, A. Dodabalapur, N. Cioffi, L. Torsi, *Mater. Today* **2011**, *14*, 424–433.
- [8] J. Nelson, *Mater. Today* **2011**, *14*, 462–470.
- [9] N. T. Kalyani, S. J. Dhoble, *Renew. Sust. Energ. Rev.* **2012**, *16*, 2696–2723.
- [10] A. C. Arias, J. D. Mackenzie, I. McCulloch, J. Rivnay, A. Salleo, *Chem. Rev.* **2010**, *110*, 3–24.
- [11] C. J. Brabec, J. A. Hauch, P. Schilinsky, C. Waldauf, *MRS Bull.* **2005**, *30*, 50–52.
- [12] J. Rivnay, S. C. B. Mannsfeld, C. E. Miller, A. Salleo, M. F. Toney, *Chem. Rev.* **2012**, *112*, 5488–5519.
- [13] A. Salleo, R. J. Kline, D. M. DeLongchamp, M. L. Chabinyc, *Adv. Mater.* **2010**, *22*, 3812–3838.
- [14] R. Noriega, J. Rivnay, K. Vandewal, F. P. Koch, N. Stingelin, P. Smith, M. F. Toney, A. Salleo, *Nat. Mater.* **2013**, *12*, 1038–1044.
- [15] T.-A. Chen, X. Wu, R. D. Rieke, *J. Am. Chem. Soc.* **1995**, *117*, 233–244.
- [16] H. Sirringhaus, P. J. Brown, R. H. Friend, M. M. Nielsen, K. Bechgaard, B. M. W. Langeveld-Voss, A. J. H. Spiering, R. A. J. Janssen, E. W. Meijer, P. Herwig, D. M. de Leeuw, *Nature* **1999**, *401*, 685–688.
- [17] R. A. Street, J. E. Northrup, A. Salleo, *Phys. Rev. B* **2005**, *71*, 165202.
- [18] W. L. Kalb, S. Haas, C. Krellner, T. Mathis, B. Batlogg, *Phys. Rev. B* **2010**, *81*, 155315.
- [19] G. Horowitz, M. E. Hajlaoui, *Adv. Mater.* **2000**, *12*, 1046–1050.
- [20] S. S. Lee, C. S. Kim, E. D. Gomez, B. Purushothaman, M. F. Toney, C. Wang, A. Hexemer, J. E. Anthony, Y.-L. Loo, *Adv. Mater.* **2009**, *21*, 3605–3609.
- [21] A. D. Carlo, F. Piacenza, A. Bolognesi, B. Stadlober, H. Maresch, *Appl. Phys. Lett.* **2005**, *86*, 263501.
- [22] W. Warta, N. Karl, *Phys. Rev. B* **1985**, *32*, 1172–1182.
- [23] M. E. Gershenson, V. Podzorov, A. F. Morpurgo, *Rev. Mod. Phys.* **2006**, *78*, 973–989.
- [24] S. Dag, L.-W. Wang, *J. Phys. Chem. B* **2010**, *114*, 5997–6000.
- [25] W. Xie, Y. Y. Sun, S. B. Zhang, J. E. Northrup, *Phys. Rev. B* **2011**, *83*, 184117.
- [26] T. J. Prosa, M. J. Winokur, J. Moulton, P. Smith, A. J. Heeger, *Macromolecules* **1992**, *25*, 4364–4372.
- [27] N. Kayunkid, S. Uttiya, M. Brinkmann, *Macromolecules* **2010**, *43*, 4961–4967.
- [28] A. Maillard, A. Rochefort, *Phys. Rev. B* **2009**, *79*, 115207.
- [29] G. R. Hutchison, Y.-J. Zhao, B. Delley, A. J. Freeman, M. A. Ratner, T. J. Marks, *Phys. Rev. B* **2003**, *68*, 035204.
- [30] N. Vukmirović, L.-W. Wang, *Nano. Lett.* **2009**, *12*, 3996–4000.
- [31] V. Coropceanu, J. Cornil, D. A. da Silva Filho, Y. Olivier, R. Silbey, J.-L. Bredas, *Chem. Rev.* **2007**, *107*, 926–952.
- [32] L. Wang, G. Nan, X. Yang, Q. Peng, Q. Lia, Z. Shuai, *Chem. Soc. Rev.* **2010**, *39*, 423–434.
- [33] A. Troisi, G. Orlandi, *Phys. Rev. Lett.* **2006**, *96*, 086601.
- [34] A. Troisi, G. Orlandi, J. E. Anthony, *Chem. Mater.* **2005**, *17*, 5024–5031.
- [35] K. D. Meisel, H. Vocks, P. A. Bobbert, *Phys. Rev. B* **2005**, *71*, 205206.
- [36] S. S. Zade, M. Bendikov, *Chem.-Eur. J.* **2008**, *14*, 6734–6741.

- [37] A. Troisi, *Chem. Soc. Rev.* **2011**, *40*, 2347–2358.
- [38] J. Ren, N. Vukmirović, L.-W. Wang, *Phys. Rev. B* **2013**, *87*, 205117.
- [39] N. Vukmirović, C. Bruder, V. M. Stojanović, *Phys. Rev. Lett.* **2012**, *109*, 126407.
- [40] M. P. Allen, D. J. Tildesley, *Computer Simulations of Liquids*, Clarendon Press, New York, USA **1987**.
- [41] N. Vukmirović, L.-W. Wang, *J. Phys. Chem. B* **2009**, *113*, 409–415.
- [42] P. Yang, E. R. Batista, S. Tretiak, A. Saxena, R. L. Martin, D. L. Smith, *Phys. Rev. B* **2007**, *76*, 241201.
- [43] G. Zhang, Y. Pei, J. Ma, K. Yin, C.-L. Chen, *J. Phys. Chem. B* **2004**, *108*, 6988–6995.
- [44] G. Zhang, J. Ma, J. Wen, *J. Phys. Chem. B* **2007**, *111*, 11670–11679.
- [45] H.-C. Yang, C.-Y. Hua, M.-Y. Kuo, Q. Huang, C.-L. Chen, *Chem. Phys. Chem.* **2004**, *5*, 373–381.
- [46] T. Qin, A. Troisi, *J. Am. Chem. Soc.* **2013**, *135*, 11247–11256.
- [47] V. Ruehle, A. Lukyanov, F. May, M. Schrader, T. Vehoff, J. Kirkpatrick, B. Baumeier, D. Andrienko, *J. Chem. Theory Comput.* **2011**, *7*, 3335–3345.
- [48] R. G. Parr, W. Yang, *Density-Functional Theory of Atoms and Molecules*, Oxford University Press, New York, USA **1989**.
- [49] N. Vukmirović, L.-W. Wang, *J. Chem. Phys.* **2008**, *128*, 121102.
- [50] A. Canning, L.-W. Wang, A. Williamson, A. Zunger, *J. Comp. Phys.* **2000**, *160*, 29–41.
- [51] L.-W. Wang, A. Zunger, *J. Chem. Phys.* **1994**, *100*, 2394–2397.
- [52] N. Vukmirović, L.-W. Wang, *J. Chem. Phys.* **2011**, *134*, 094119.
- [53] T. Liu, A. Troisi, *Adv. Funct. Mater.* **2013**, *24*, 925–933.
- [54] D. P. McMahon, A. Troisi, *Chem. Phys. Lett.* **2009**, *480*, 210–214.
- [55] N. Vukmirović, L.-W. Wang, *J. Phys. Chem. B* **2011**, *115*, 1792–1797.
- [56] D. H. Dunlap, P. E. Parris, V. M. Kenkre, *Phys. Rev. Lett.* **1996**, *77*, 542–545.
- [57] B. Baumeier, F. May, C. Lennartz, D. Andrienko, *J. Mater. Chem.* **2012**, *22*, 10971–10976.
- [58] B. Kramer, A. MacKinnon, *Rep. Prog. Phys.* **1993**, *56*, 1469–1564.
- [59] N. Vukmirović, *Phys. Chem. Chem. Phys.* **2013**, *15*, 3543–3551.
- [60] J. M. Granadino-Roldan, N. Vukmirović, M. Fernandez-Gomez, L.-W. Wang, *Phys. Chem. Chem. Phys.* **2011**, *13*, 14500–14509.
- [61] D. L. Cheung, D. P. McMahon, A. Troisi, *J. Am. Chem. Soc.* **2009**, *131*, 11179–11186.
- [62] S. Fratini, S. Ciuchi, *Phys. Rev. Lett.* **2009**, *103*, 266601.
- [63] S. Ciuchi, S. Fratini, *Phys. Rev. Lett.* **2011**, *106*, 166403.
- [64] B. L. M. Hendriksen, F. Martin, Y. Qi, C. Mauldin, N. Vukmirović, J. Ren, H. Wormeester, A. J. Katan, V. Altoe, S. Aloni, J. M. J. Frechet, L.-W. Wang, M. Salmeron, *Nano Lett.* **2011**, *11*, 4107–4112.
- [65] A. B. Chwang, C. D. Frisbie, *J. Appl. Phys.* **2001**, *90*, 1342–1349.
- [66] J. Chen, C. K. Tee, M. Shtein, J. Anthony, D. C. Martin, *J. Appl. Phys.* **2008**, *103*, 114513.
- [67] J. Rivnay, L. H. Jimison, J. E. Northrup, M. F. Toney, R. Noriega, S. Lu, T. J. Marks, A. Facchetti, A. Salleo, *Nat. Mater.* **2009**, *8*, 952–958.
- [68] S. Verlaak, V. Arkhipov, P. Heremans, *Appl. Phys. Lett.* **2003**, *82*, 745–747.
- [69] G. Horowitz, *Adv. Funct. Mater.* **2003**, *13*, 53–60.
- [70] S. Verlaak, P. Heremans, *Phys. Rev. B* **2007**, *75*, 115127.
- [71] M. Mladenović, N. Vukmirović, I. Stanković, *J. Phys. Chem. C* **2013**, *117*, 15741–15748.
- [72] L. G. Kaake, P. F. Barbara, X.-Y. Zhu, *J. Phys. Chem. Lett.* **2010**, *1*, 628–635.
- [73] G. Nan, Z. Li, *Org. Electron.* **2011**, *12*, 2198–2206.
- [74] J. L. Brédas, J. P. Calbert, D. A. da Silva Filho, J. Cornil, *Proc. Natl. Acad. Sci. U. S. A.* **2002**, *99*, 5804–5809.
- [75] H. Bassler, *Phys. Status Solidi B* **1993**, *175*, 15–56.
- [76] P. M. Borsenberger, L. Pautmeier, H. Bassler, *J. Chem. Phys.* **1991**, *94*, 5447–5454.
- [77] S. D. Baranovskii, *Phys. Status Solidi B* **2014**, *251*, 487–525.
- [78] R. Coehoorn, W. F. Pasveer, P. A. Bobbert, M. A. J. Michels, *Phys. Rev. B* **2005**, *72*, 155206.
- [79] A. Miller, E. Abrahams, *Phys. Rev.* **1960**, *120*, 745–755.
- [80] A. Lukyanov, D. Andrienko, *Phys. Rev. B* **2010**, *82*, 193202.
- [81] S. Marianer, B. I. Shklovskii, *Phys. Rev. B* **1992**, *46*, 13100–13103.
- [82] F. Jansson, S. D. Baranovskii, F. Gebhard, R. Osterbacka, *Phys. Rev. B* **2008**, *77*, 195211.
- [83] N. Vukmirović, L.-W. Wang, *Phys. Rev. B* **2010**, *81*, 035210.
- [84] H. Cordes, S. D. Baranovskii, K. Kohary, P. Thomas, S. Yamasaki, F. Hensel, J.-H. Wendorff, *Phys. Rev. B* **2001**, *63*, 094201.
- [85] G. Juška, K. Genevičius, K. Arlauskas, R. Österbacka, H. Stubbs, *Phys. Rev. B* **2002**, *65*, 233208.
- [86] V. Ambegaokar, B. I. Halperin, J. S. Langer, *Phys. Rev. B* **1971**, *4*, 2612–2620.
- [87] C. Tanase, E. J. Meijer, P. W. M. Blom, D. M. de Leeuw, *Phys. Rev. Lett.* **2003**, *91*, 216601.
- [88] N. I. Craciun, J. Wildeman, P. W. M. Blom, *Phys. Rev. Lett.* **2008**, *100*, 056601.
- [89] J.-D. Picon, M. N. Bussac, L. Zuppiroli, *Phys. Rev. B* **2007**, *75*, 235106.
- [90] Y.-C. Cheng, R. J. Silbey, *J. Chem. Phys.* **2008**, *128*, 114713.
- [91] F. Ortman, F. Bechstedt, K. Hannewald, *Phys. Rev. B* **2009**, *79*, 235206.
- [92] K. Hannewald, V. M. Stojanovic, J. M. T. Schellekens, P. A. Bobbert, G. Kresse, J. Hafner, *Phys. Rev. B* **2004**, *69*, 075211.
- [93] H. Ishii, K. Honma, N. Kobayashi, K. Hirose, *Phys. Rev. B* **2012**, *85*, 245206.
- [94] P. V. Parandekar, J. C. Tully, *J. Chem. Phys.* **2005**, *122*, 094102.
- [95] J. C. Tully, *J. Chem. Phys.* **1990**, *93*, 1061–1071.
- [96] L. Wang, D. Beljonne, *J. Phys. Chem. Lett.* **2013**, *4*, 1888–1894.
- [97] N. F. Mott, E. A. Davis, *Electronic Processes in Non-Crystalline Materials*, Clarendon Press, New York, USA **1979**.
- [98] S. A. Choulis, Y. Kim, J. Nelson, D. D. C. Bradley, M. Giles, M. Shkunov, I. McCulloch, *Appl. Phys. Lett.* **2004**, *85*, 3890–3892.